Strong Pressure Waves in Air-Breathing Engines

V.E. Haloulakos*
McDonnell Douglas Astronautics Company, Huntington Beach, California

Fuel ingestion, damage from foreign objects, or a simple high-pressure compressor stall can cause strong pressure waves in air-breathing engines. These waves travel at sonic and supersonic velocities throughout all engine compartments, where they may cause structural damage. A computer program for unsteady compressible gas flow has been used to analyze and evaluate the transient flow phenomena caused by these waves. Starting with a steady-state gas flow input defining nominal pressures, velocities, and temperatures, a pressure pulse simulating an explosion is placed at some specified location. The program then computes the variations of all the flow parameters as a function of time at every point throughout the engine. The program is modularly constructed and can simulate any engine gas flow geometry by means of judicious numbering and connection of the various modules. The program has been successfully used to assess the severity of high-pressure waves in numerous cases and has correlated very well with experimental data.

Nomenclature

A, B = Riemann invariants
a = sonic velocity
c_p = specific heat at constant pressure
c_v = specific heat at constant volume
E = energy
E_f = energy dissipation function
f_i = body force
F_f = friction force
h = internally generated heat
p = pressure
q_i = heat flux
R = gas constant
s = entropy
S = flow area
t = time
T = temperature
u = fluid velocity
x = space variable
α, β = right and left running characteristics
γ = specific heat ratio
δ_{ij} = Kronecker delta
σ_{ij} = stress tensor, $= -p\delta_{ii} + \tau_{ij}$
τ_{ij} = shear stress tensor
ϕ = special function

Note: all units are in lb, ft, s, and °R.

Introduction

STRONG pressure waves in turbofan, turbojet, and other ducted engines can be caused by a variety of events, the most common of which are high-pressure compressor (HPC) stalls or internal explosions following fuel ingestion. Regardless of their source or origin, these pressure waves propagate throughout the engine compartments, resulting in high local pressures, rapid flow reversals, and possibly structural failures.

Both the design and installation of engines in airplanes, therefore, must include an evaluation of these transient flow phenomena. Evaluations can be made by test, analysis, or combinations thereof. Engine testing alone is very expensive, time-consuming, and quite often inconclusive, because it only provides information for the specific engine tested. A better approach is to use a transient fluid analysis, i.e., a time-dependent model wth rapid flow reversal capability to evaluate the problems and then to conduct only a small number of specified tests in order to validate and/or improve the analysis. When a good correlation has been obtained, the analysis can then be used in lieu of testing for evaluating any air-breathing engine in question. This will always result in more information than testing; it will cost less; and it will save time.

This paper discusses the use of a mathematical formulation and computer model for evaluating and assessing strong pressure wave phenomena in air-breathing engines.

The computational scheme uses the basic equations of unsteady compressible fluid flow, and the solution is obtained via the method of characteristics. The model can account for friction, heat-transfer, and energy dissipation (or addition) effects. The computer program is modularly constructed, permitting gas flow systems with almost any configuration to be analyzed. Modules can account for constant and/or variable area ducts and boundary conditions such as tees, crosses, open and closed ends, step area changes, variable area orifices, valves, and infinite and finite reservoirs. By judicious selection and numbering of modules, the physical configuration of any air-breathing engine can be simulated. The equations and their method of solution are shown in the Appendix. Additional details can be found in Refs. 1-3.

Discussion

A common phenomenon when strong pressure waves occur in air-breathing engines is the spewing of flame out of the engine inlet—a clear indication of flow velocity reversal. This particular phenomenon appears to be peculiar to wing-mounted engines and is not observed in the tail-mounted engines of the widebodied jets that are currently flying. In the case of tail-mounted engines, compressor stalls and engine flameouts result in the flame spewing out the aft end only. The length, diameter, and flow conditions of the tail-mounted inlet engine duct are responsible for the difference observed at the two engine locations. The strength of the pressure pulse required to reverse the flow in ducts, such as those found in the tail-mounted engines of the widebodied jets, would probably have more serious structural effects in their region of occurrence.

The method of analysis and the associated computer program described in Ref. 1 were used in three distinct cases:

Presented as Paper 81-1475 at the AIAA/SAE/ASME 17th Joint Propulsion Conference, Colorado Springs, Colo., June 27-29, 1981; submitted Aug. 12, 1981; revision received July 27, 1982.

*Senior Engineer/Scientist, Propulsion Department. Associate Fellow AIAA.

one involving pressure waves caused by internal explosions following damage by a foreign object (FOD), and two caused by fuel ingestion. Correlation of analytic data to test data is excellent.

FOD Case

During a ground test program simulating actual or expected FOD-caused phenomena, explosions were caused and the pressure wave propagations were measured. The results of a typical ground test, shown in Fig. 1, indicate two pressure wave peaks at two different locations in the engine, at two different times. The questions that must be answered, however, are where did the pressure wave originate, and how strong was it at that point?

To answer these questions the engine was simulated using the techniques described in Ref. 1. The ducting configuration is shown in Fig. 2. The main elements are the variable area duct simulating the high-pressure compressor (HPC), the inlet duct at one end, and a long duct at the other end that serves to isolate the compressor from the engine exhaust hardware and geometry. The figure also shows the steady-state pressure curve and the magnitude and location of the input pressure spike. The results of the simulation are shown in the next two figures. Figure 3 shows a 245-psig pressure wave, traveling toward the combustor, hitting test point 1 at 0.35 ms after the pressure pulse application. Figure 4 shows a 95-psig pressure wave hitting the HPC inlet (test point 2) at time 2.5 ms, i.e., precisely 2.15 ms after the 245-psig wave hit test point 1.

The program computed the pressure peaks and the times of occurrence at every point throughout the engine. It also indicated that flow reversal should occur in the engine inlet and flame should spew out of the inlet 5.8 ms after the explosion. This was verified by the test.

Fuel Ingestion Case

Use of the program was expanded to simulate the entire turbofan engine configuration in order to trace the paths of pressure waves caused by fuel ingestion. Ground test programs have verified that fuel ingestion in the HPC areas[4] can cause internal explosions that travel throughout the engine compartments.

Specifically, the program was used to assess and evaluate the problems that may be encountered in the tail-mounted,

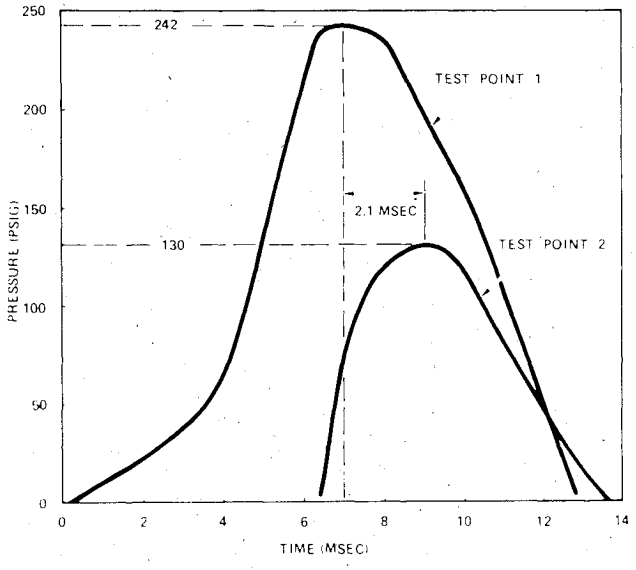

Fig. 1 Test engine pressure pulse data.

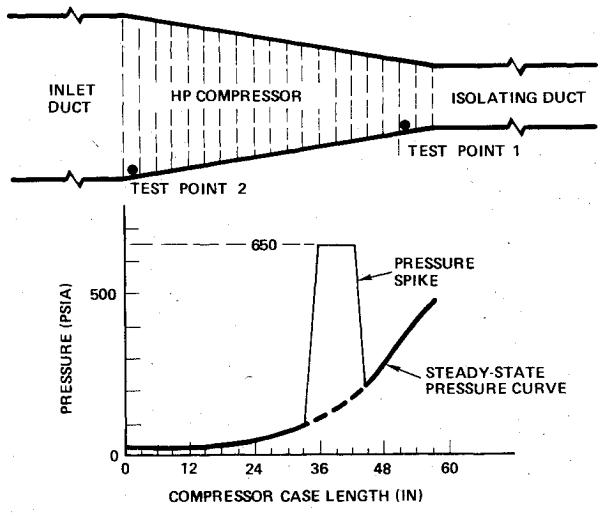

Fig. 2 High-pressure compressor and interconnecting ducts.

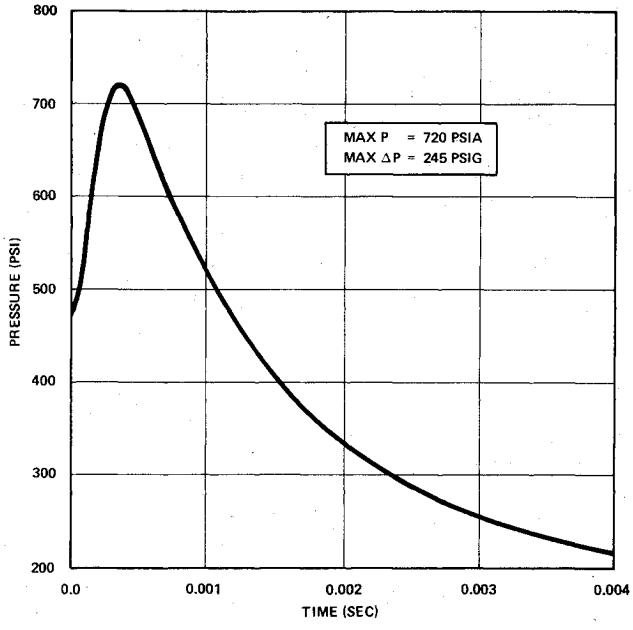

Fig. 3 Pressure transients for test point 1.

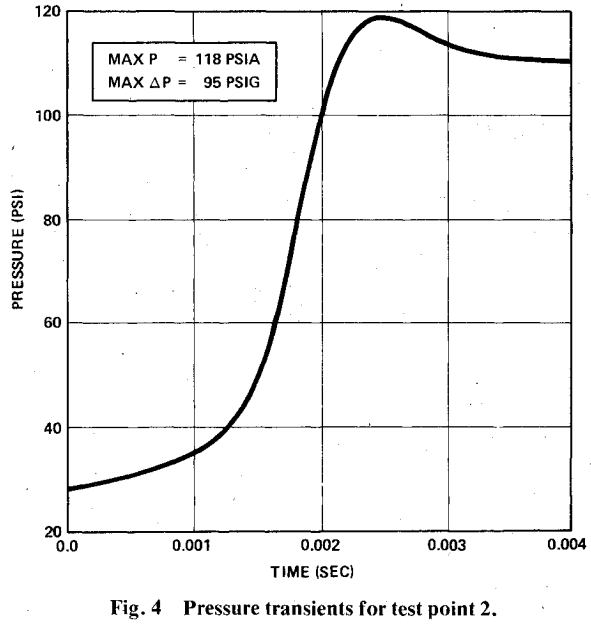

Fig. 4 Pressure transients for test point 2.

high-thrust turbofan engines. The distinctive features of these engines are long inlet ducts, high bypass ratio, and high thrust, which are accompanied by high air flows. A scale schematic of such an engine is shown in Fig. 5.

The engine was modeled in a modular fashion, shown in Fig. 6, with each component described in terms of its length and cross-sectional or net flow area. The steady-state flowfield was also input, along with a 500-psia pressure spike in the HPC. As the pressure and temperature increase in the combustor, a pressure wave travels in both the upstream and downstream directions. At the region around the fan the pressure wave splits into two parts: one goes into the inlet duct and the other into the fan duct. The strength of each part of this traveling wave is primarily determined by the cross-sectional area of the ducts. The wave that enters the inlet duct is weaker than that in the fan duct largely because of the significant difference in cross-sectional area.

These pressure waves travel in the media at the local sonic velocity. The net wave velocity relative to the engine hardware, however, is the algebraic sum between local sonic and local flow velocities.

In the cases studied here, the net wave velocities are approximately 450 and 1500 ft/s in the inlet and the fan ducts, respectively. Therefore, before the wave traverses 1 ft up the inlet duct, it will have traversed 3 ft down the fan duct. The fan duct being approximately 6 ft long, the pressure wave will hit the fan nozzle exit by the time it has moved 2 ft up the inlet duct. The next event is an expansion wave moving up the fan duct exit relieving the pressure. Thus, the pressure rise is greater in the fan duct, and it occurs earlier because of the local flow velocity effects.

The predicted pressure peaks along the fan duct length and the times of their occurrences are summarized in Fig. 7. A more meaningful form of the pressure data, however, is the actual time history at each point. Figures 8-10 show the pressure-time histories of three points along the fan duct. The attenuation, caused by wall friction as the pressure wave travels down the duct, is evident.

The pressure-time history at a point in the inlet duct is shown in Fig. 11, which indicates that the maximum pressure is approximately 15 psia. This pressure wave will travel up the inlet duct, but it will not raise pressures significantly. Thus, it is concluded that pressure waves originating in the HPC or combustor regions would not cause any problems in the inlet duct. The region of concern would more than likely be the fan duct area, where higher pressures are experienced.

These conclusions as to the location and the degree of severity of the problems direct the designer to the proper area of concern. He can use this information to prevent such problems from occurring. In order to have confidence in these analytical predictions, however, correlation with test data is always desirable and very often required.

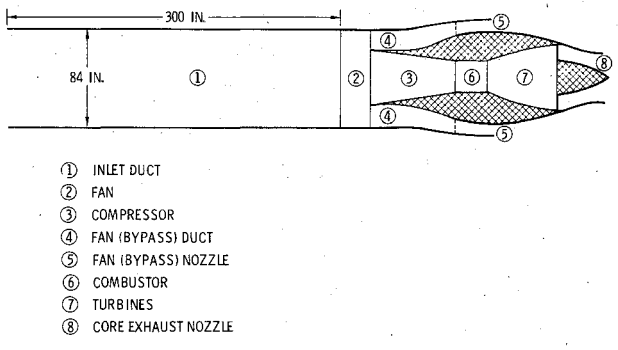

Fig. 5 Turbofan engine schematic.

Correlation with Test Data

The predictions of the program were validated by the successful simulation of test data obtained from the Naval Weapons Center (NWC), China Lake.[4]

Actual engines, operating with realistic airflows and under proper environmental conditions, were made to ingest fuel. Instrumentation recorded the explosions and the propagation of the ensuing pressure waves. A schematic of a typical test engine is shown in Fig. 12. It should be noted that it is smaller than the large turbofan shown in Fig. 5; the length of the inlet duct is a little longer, but its diameter is substantially smaller.

For the purpose of correlating the computer data, three fast-response transducers located at three key points were identified. Several pressure pulses were applied at the HPC-to-combustor interface and the pressure wave peaks

Table 1 Parametric pressure simulation data, psia

	Combustor	PSFK	PSIAK
Computed pressures	930	330	150
	620	238	105
	580	204	95
	220[a]	85	24
Test data[b]		190	93

[a] Simple compressor stall, i.e., no added pressure pulse. [b] Courtesy of NWC, China Lake.

Table 2 Turbofan engine pressure data correlation, psia

	Combustor	PSFK	PSIAK	PSIBK
Max pressures,				
Measured[a]	>540	190	93	64
Computed	575	194	82	72

[a] Courtesy of NWC, China Lake.

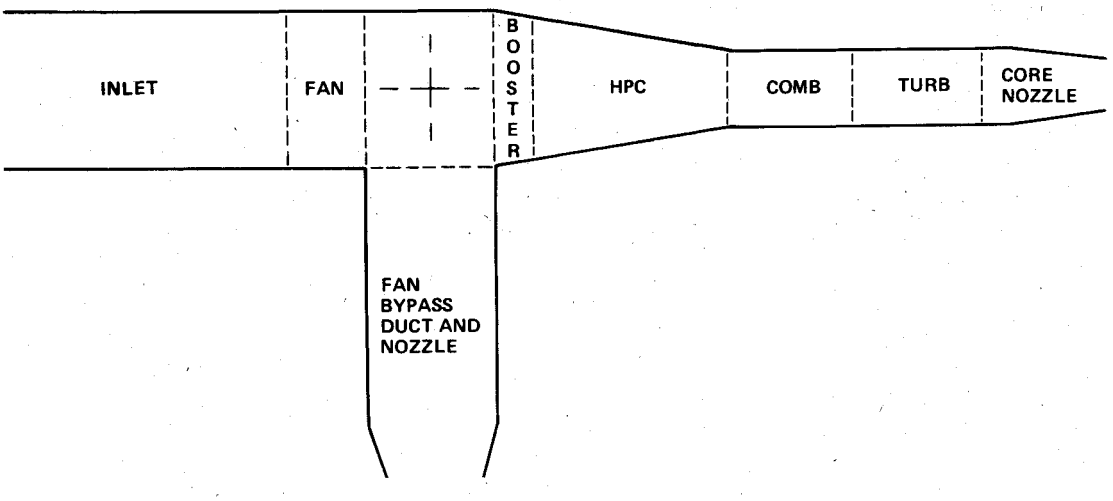

Fig. 6 Wave dynamics simulation of a turbofan engine.

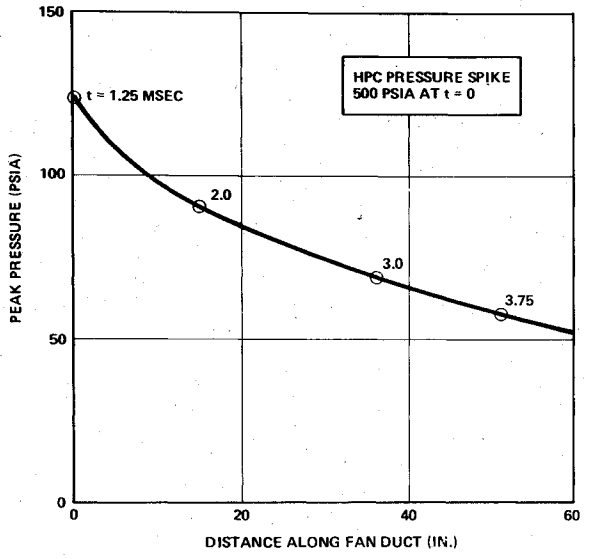

Fig. 7 Fan duct pressures.

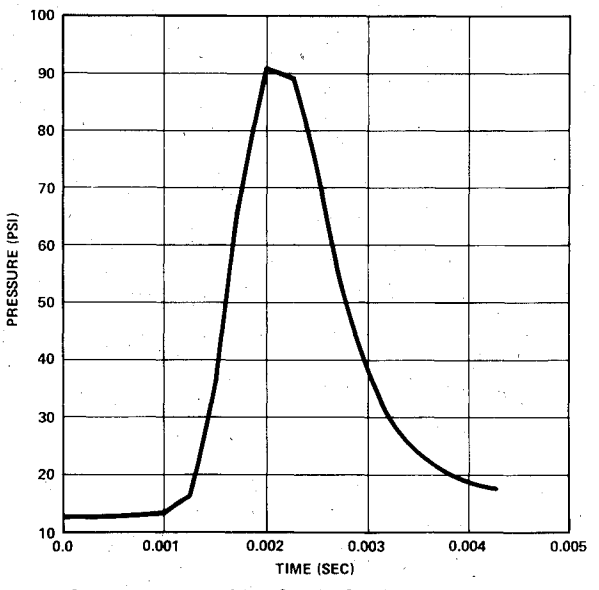

Fig. 8 Pressure transients for the fan duct quarter point.

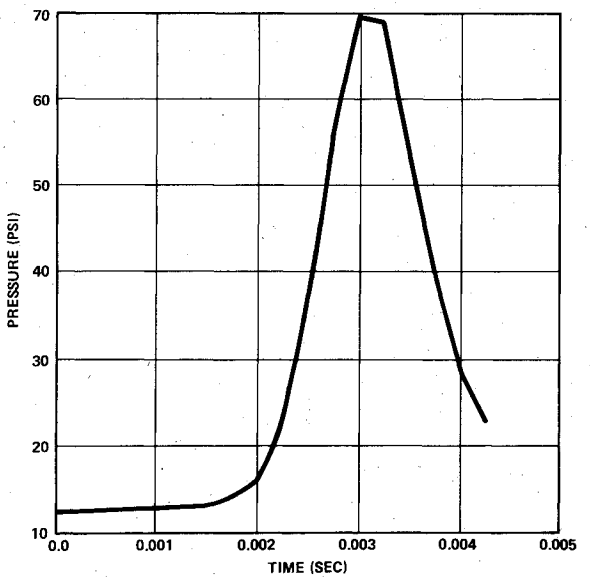

Fig. 9 Pressure transients for the fan duct midpoint.

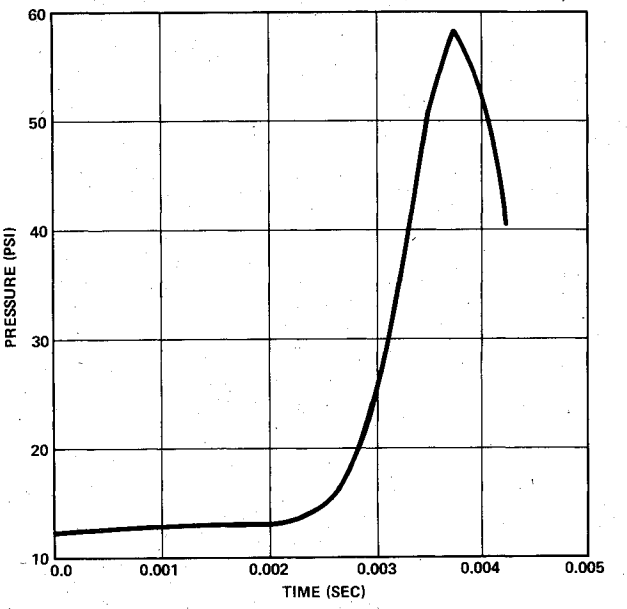

Fig. 10 Pressure transients for the fan duct three-quarter point.

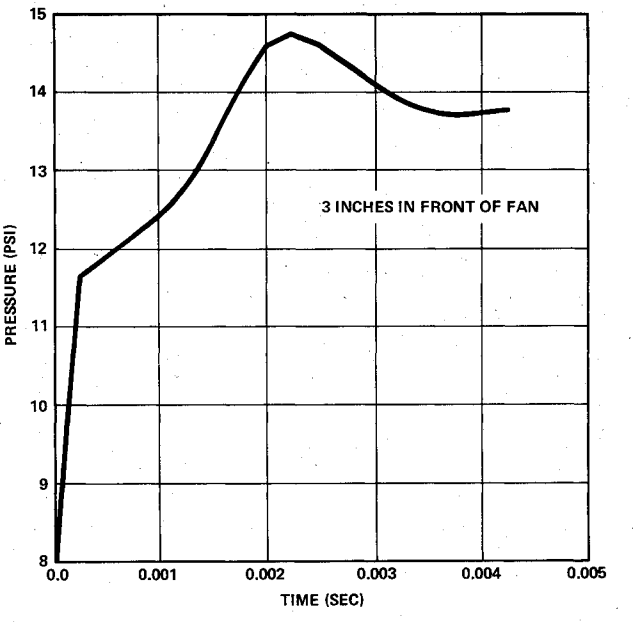

Fig. 11 Pressure transients for the inlet duct.

calculated at the first two test locations, PSFK and PSIAK; the results are shown in Table 1. A comparison with the test data reveals that a pressure pulse slightly less than 580 psia would adequately simulate the test data at the two test points. A 575-psia pressure pulse was then applied, and the program was allowed to run until the pressure wave also hit the third test point, PSIBK. The results are summarized in Table 2. The time-history plots of the pressures at these three points are shown in Figs. 13-15. The pressure wave also traveled down the fan duct. The pressure-time histories at two different stations are shown in Figs. 16 and 17.

In the ground tests, flame was observed to spew out of the front of the inlet duct. This definitely implies flow velocity reversal in the inlet duct. This was also computed by the program, as shown in Fig. 18, for test point PSIBK. This is a distinct variation from the case of the large turbofan engine discussed earlier, a clear indication that the duct geometry, diameter in this case, is a major factor in pressure pulse propagation and behavior.

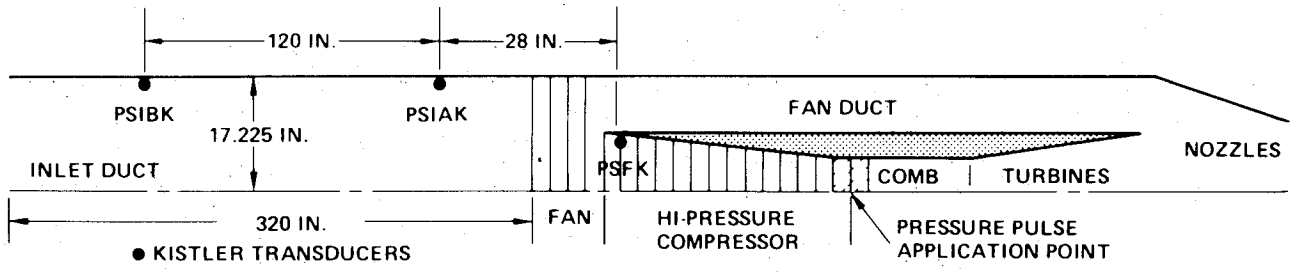

Fig. 12 Test turbofan engine and fast-response pressure data points. (Courtesy of NWC, China Lake.)

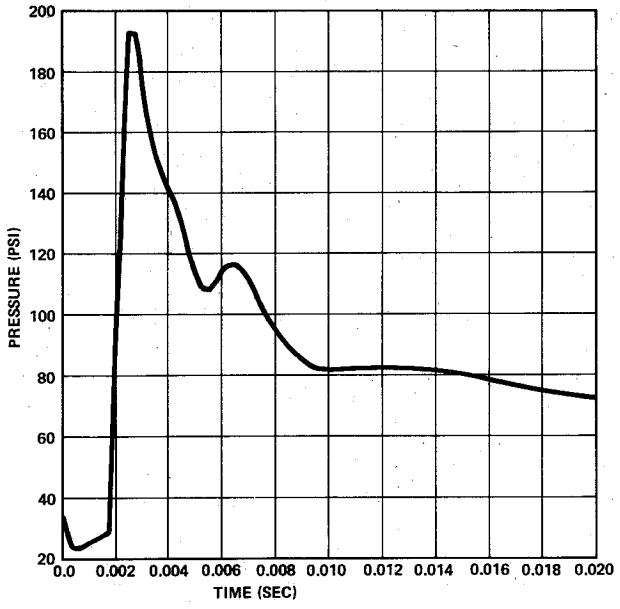

Fig. 13 HPC inlet pressure transients (location PSFK).

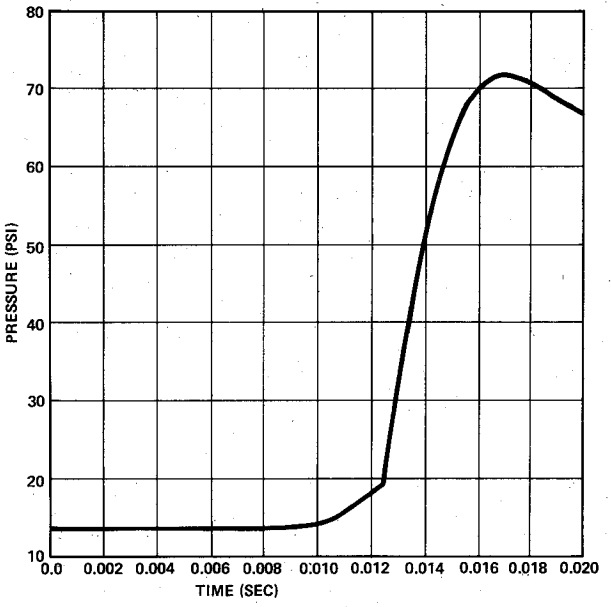

Fig. 15 Pressure transients for inlet duct test point PSIBK.

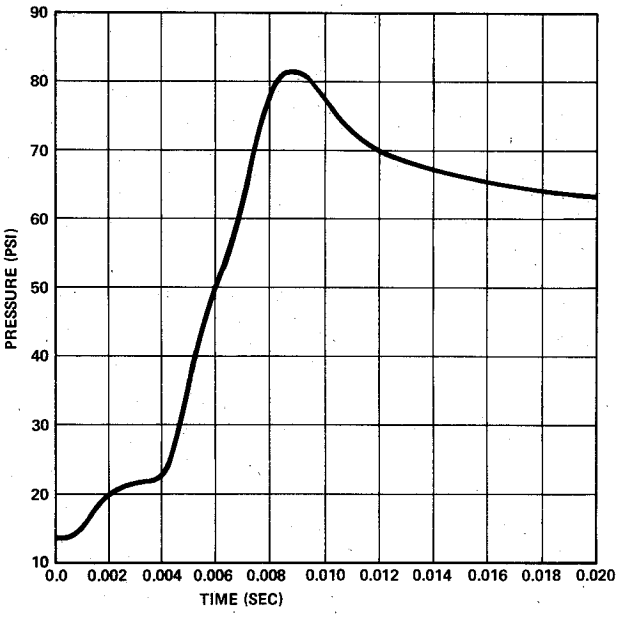

Fig. 14 Pressure transients for inlet duct test point PSIAK.

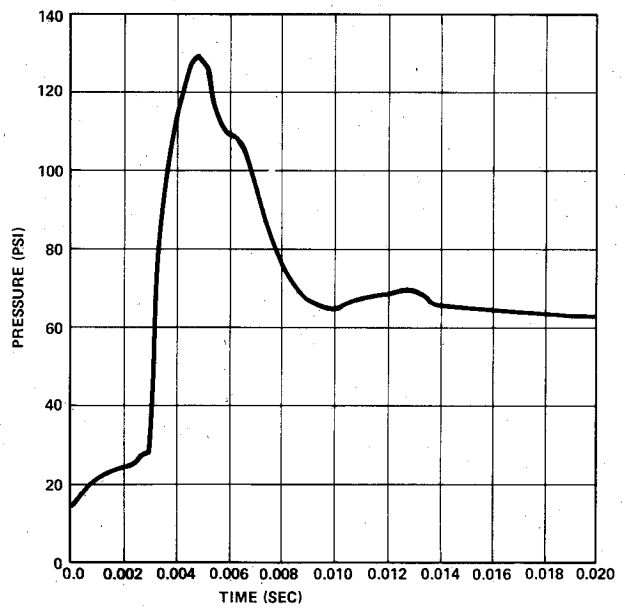

Fig. 16 Inlet duct pressure transients at the fan.

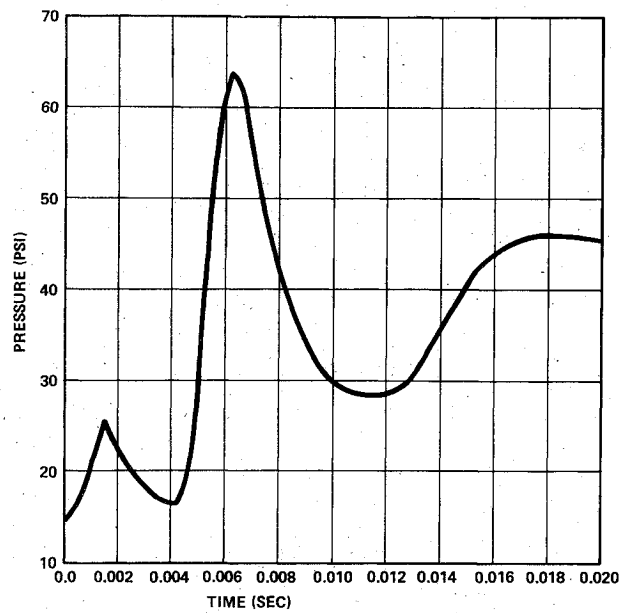

Fig. 17 Pressure transients 6 ft down the fan duct.

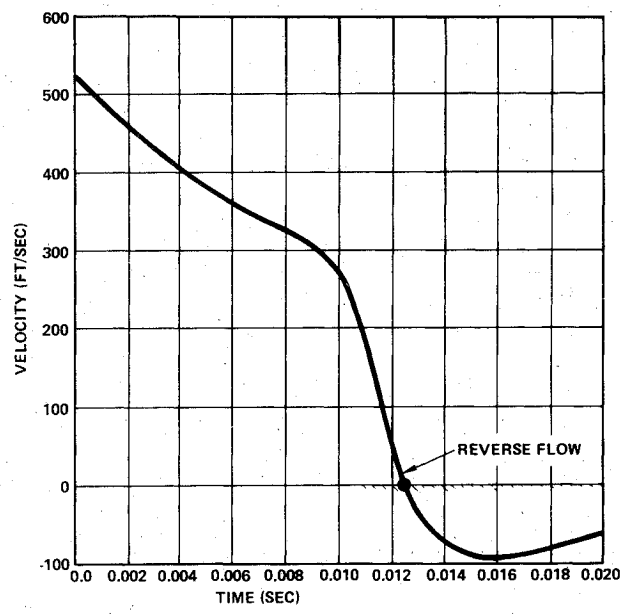

Fig. 18 Flow velocity transients for inlet duct test point PSIBK.

Conclusions

The close correlation between the computed and measured pressure wave data in the cases discussed verified that the program can be used as a reliable design tool in the evaluation of pressure waves in turbofan engines, and that its predictions can be used with confidence for design purposes. Its best use is to identify and assess problem areas in candidate designs before any actual design is initiated. It can be used in lieu of hardware testing to evaluate candidate systems and to extrapolate design data from one system to another. In fact, it gives far more information than tests do; e.g., data on flow velocity, density, etc., are not easily obtainable from tests. Judicious use of this program can identify the most viable and promising designs, which can be subjected to testing if necessary. This can result in substantial cost savings.

Appendix: Analytical Formulation

The mathematical formulation of the problem, the underlying assumptions, and the method of solution are as follows.

Basic equations of motion:

Continuity

$$\frac{\partial}{\partial t}(\rho S)+\frac{\partial}{\partial x_i}(\rho S u_i)=0 \tag{A1}$$

Momentum

$$\rho\left(\frac{\partial u_i}{\partial t}+u_j\frac{\partial u_i}{\partial x_j}\right)=\rho f_i+\frac{\partial \sigma_{ij}}{\partial x_j} \tag{A2}$$

Energy

$$\rho\frac{\mathrm{d}E}{\mathrm{d}t}=\sigma_{ij}\frac{\partial u_i}{\partial x_j}+\frac{\partial q_i}{\partial x_i}+\rho h \tag{A3}$$

State

$$p=\rho RT \tag{A4}$$

The assumptions are: 1) variable area rigid duct, 2) no body forces, 3) one-dimensional flow, 4) viscous fluid, 5) no internally generated heat, 6) constant specific heats and molecular weight.

Introducing these assumptions the basic equations become

$$\frac{\partial \rho}{\partial t}+u\frac{\partial \rho}{\partial x}+\rho\frac{\partial u}{\partial x}+\frac{\rho}{S}\left(\frac{\partial S}{\partial t}+u\frac{\partial S}{\partial x}\right)=0 \tag{A5}$$

$$\frac{\partial u}{\partial t}+u\frac{\partial u}{\partial x}+\frac{1}{\rho}\frac{\partial p}{\partial x}+F_f=0 \tag{A6}$$

$$\left(\frac{\partial p}{\partial t}+u\frac{\partial p}{\partial x}\right)-a^2\left(\frac{\partial \rho}{\partial t}+u\frac{\partial \rho}{\partial x}\right)-(\gamma-1)\left[\frac{\partial q}{\partial x}+E_f\right]=0 \tag{A7}$$

$$p=\rho RT \tag{A8}$$

A solution by the method of characteristics leads to

$$\left[\frac{\partial p}{\partial t}+(u\pm a)\frac{\partial p}{\partial x}\right]\pm a\rho\left[\frac{\partial u}{\partial t}+(u\pm a)\frac{\partial u}{\partial x}\right]\pm a\rho F_f-\left[(\gamma-1)\right]\left[\frac{\partial q}{\partial x}+E_f\right]+\frac{\rho a^2}{S}\left[\frac{\partial S}{\partial t}+u\frac{\partial S}{\partial x}\right]=0 \tag{A9}$$

which results in the following set of equations

$$\frac{\mathrm{d}p}{\mathrm{d}t}+a\rho\frac{\mathrm{d}u}{\mathrm{d}t}+a\rho F_f-(\gamma-1)\left(\frac{\partial q}{\partial x}+E_f\right)+\frac{\rho a^2}{S}\frac{\mathrm{d}S}{\mathrm{d}t}=0$$

$$\text{along}\quad \frac{\mathrm{d}x}{\mathrm{d}t}=u+a \tag{A10}$$

$$\frac{\mathrm{d}p}{\mathrm{d}t}-a\rho\frac{\mathrm{d}u}{\mathrm{d}t}-a\rho F_f-(\gamma-1)\left(\frac{\partial q}{\partial x}+E_f\right)+\frac{\rho a^2}{S}\frac{\mathrm{d}S}{\mathrm{d}t}=0$$

$$\text{along}\quad \frac{\mathrm{d}x}{\mathrm{d}t}=u-a \tag{A11}$$

and finally

$$\frac{\mathrm{d}p}{\mathrm{d}t}-a^2\frac{\mathrm{d}\rho}{\mathrm{d}t}-(\gamma-1)\left(\frac{\partial q}{\partial x}+E_f\right)=0\quad\text{along}\quad\frac{\mathrm{d}x}{\mathrm{d}t}=u \tag{A12}$$

If the heat-transfer and energy dissipation functions are expressed on a per-unit-mass basis and if the pressure is expressed in terms of the density and entropy, Eq. (A12)

becomes

$$\frac{ds}{dt} = \frac{R\rho}{p}\left[\frac{\partial q}{\partial x} + E_f\right] \tag{A13}$$

which represents a continuous variation in entropy along the fluid streamlines.

Introducing a new function ϕ, such that

$$d\phi = \frac{dp}{d\rho} + C\,ds \tag{A14}$$

and utilizing the basic thermodynamic relationships

$$p = f(s)\rho^{\gamma} \tag{A15}$$

$$ds = c_v \frac{dT}{T} - R\frac{d\rho}{\rho} \tag{A16}$$

Eqs. (A10) and (A11) become

$$dA = G\,dt + C\,ds \quad \text{for} \quad dx = \alpha\,dt \tag{A17}$$

$$dB = N\,dt + C\,ds \quad \text{for} \quad dx = \beta\,dt \tag{A18}$$

where

$$G = -F_f + \frac{\gamma - 1}{a}\left(\frac{\partial q}{\partial x} + E_f\right) - \frac{a}{S}\frac{dS}{dt} \tag{A19}$$

$$N = F_f + \frac{\gamma - 1}{a}\left(\frac{\partial q}{\partial x} + E_f\right) - \frac{a}{S}\frac{dS}{dt} \tag{A20}$$

$$C = \frac{a}{c_p(\gamma - 1)} \tag{A21}$$

$$\phi = \left(\frac{2}{\gamma - 1}\right)a \tag{A22}$$

$$A = \phi + u \tag{A23}$$

$$B = \phi - u \tag{A24}$$

$$\alpha = u + a \tag{A25}$$

$$\beta = u - a \tag{A26}$$

Equations (A13), (A17), and (A18) form the basis of the computation technique by utilizing the characteristic grid shown in Fig. A1 and computing the various coefficients via Eqs. (A19-A26). Initial conditions are input along the entire boundary, i.e., for all values of x the flow is completely specified, and via the use of the above-cited equations, a new set of flow parameters are computed a time step Δt later. The program uses interpolation routines to obtain the values of the flow variables at stations x_α, x_u, and x_β via the use of the data at the adjacent points, x_{i-1}, x_i, and x_{i+1}. The entropy increase is calculated along the streamline, and the remainder of the flow variables are computed along the α and β characteristics. The possibility of any of the points (x_u, x_α, or x_β) falling outside the prescribed space interval is precluded by the use of the Courant-Friedrichs-Lewy stability criteria, which simply state that no wave travels more than Δx in any given Δt, mathematically given by

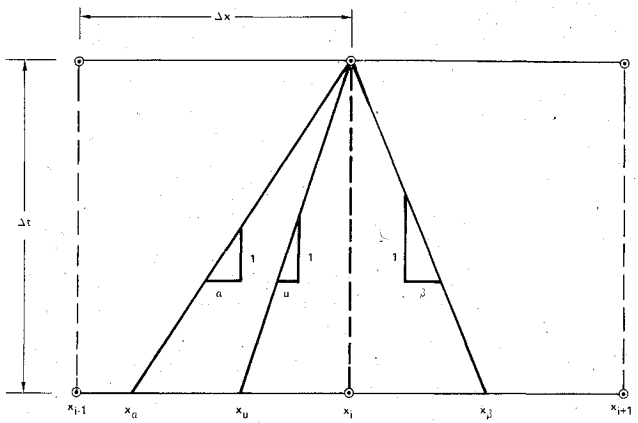

Fig. A1 Basic characteristics computation grid net.

$$\Delta t \le \frac{\Delta x}{|u| + a} \tag{A27}$$

The actual procedure is to firmly establish the space increment Δx, enter an estimated Δt, and allow the program to change it if necessary, as dictated by the maximum values of the flow velocity u and the sonic velocity a.

References

[1] Haloulakos, V.E. and Smith, M.S., "High Frequency Wave Dynamics for Compressible Flow Networks," McDonnell Douglas Astronautics Co., Huntington Beach, Calif., Rept. MDC G4874, Aug. 1973.

[2] Haloulakos, V.E., "The 'Wave Dynamics' Program and its Use in Solving Critical Unsteady Compressible Flow Problems," AIAA Paper 80-1447, Snowmass, Colo., July 1980.

[3] Haloulakos, V.E., "Wave Dynamics of Unsteady Compressible Flow Networks," *Journal of Spacecraft and Rockets,* Vol. 18, Sept.-Oct. 1981, pp. 435-439.

[4] Communications and Briefings with Technical Personnel, Systems Survivability and Lethality Division, Naval Weapons Center, China Lake, Calif., April 1976-Aug. 1980.